ORIGINAL RESEARCH

Evaluating the multiple benefits offered by ion mobility-mass spectrometry in oil and petroleum analysis

Jérémie Ponthus · Eleanor Riches

Abstract Ion mobility-mass spectrometry is starting to be considered as a useful tool in the deconvolution of complex oil and petroleum samples. While ultrahigh resolution mass spectrometry is the incumbent technology in this field, ion mobility offers complementary information related to species size and shape, and also the ability to resolve structural isomers. In this work, a sample of the resins portion of the Saturates, Aromatics, Resins, and Asphaltenes (SARA) fractions of crude oil was analysed using an orthogonal acceleration quadrupole time-of-flight mass spectrometer (oa-QToF MS) that incorporates a travelling wave ion mobility spectrometry (TWIMS) region. The ion mobility data were compared with previously acquired ultrahigh resolution Fourier transform ion cyclotron resonance mass spectrometry (FT-ICR MS) data and various nitrogen containing families were identified. Ion mobility data were processed in the typical way for the oil and petroleum industry; and the use of high resolution exact mass coupled with mobility data to provide enhanced species resolution was examined. Double bond equivalence (DBE) and carbon number groups were identified using patterns in the ion mobility data, which demonstrated the utility of ion mobility for discovering species relationships within the crude oil sample. The ability to calibrate the ion mobility cell and generate sizes for the detected ions was also recognised as potentially having particular value for the implementation of conversion or hydrotreatment processes in the oil industry.

Keywords Travelling wave ion mobility spectrometry (TWIMS) · QToF MS · Crude oil · SARA fraction · Resins

J. Ponthus
IFP Energies Nouvelles, Rond-point de l'échangeur de Solaize–BP 3, 69360 Solaize, France

E. Riches (✉)
Waters Corporation, Atlas Park, Simonsway, Manchester M22 5PP, UK
e-mail: eleanor_riches@waters.com

Introduction

The challenges presented by the compositional analysis of crude oil and petroleum-related samples were recognised as far back as the 1950s [1] and 1960s [2]. The extreme complexity of typical samples in this field requires analytical instrumentation that employ strategies to deconvolute this level of complexity. Meeting these analytical challenges has evolved into a state-of-the-art science dubbed petroleomics [3–7]—the comprehensive characterisation of oil and petroleum samples. Several different data visualisation techniques are used to display and interact with oil and petroleum data, an example of which is the Kendrick plot [8–10]. These plots represent graphical heat maps of key information related to compound classes within the sample of interest. Typically, bespoke software is used to plot m/z on the x-axis and Kendrick mass defect (a value related to a species' nominal mass and its exact mass defect) on the y-axis. The m/z values correspond to carbon number, or degree of alkylation; the Kendrick mass defect values correspond to double bond equivalence (DBE), or degree of aromaticity. This type of data visualisation provides valuable information to chemists and engineers who analyse and evaluate crude oils.

Currently, one of the key tools for today's analytical chemists working in this field is Fourier transform ion cyclotron resonance mass spectrometry (FT-ICR MS) [11], due to its ultrahigh mass resolving capabilities [12]. Crude oil contains many isobaric species that differ in mass, in some cases, by less than 10 mDa [5, 13]. The bulk of the components in oil comprise hydrocarbon species, some of which incorporate heteroatoms, resulting in the possibility of having many different species occurring at each nominal mass. Hence, the application of high and ultrahigh mass resolution to the challenge can bring benefits, and help to characterise and understand the complex sample.

Utilising ultrahigh mass resolution is just one way of approaching the challenges of complex mixture analysis. However, this cannot address the separation of species that are truly isomeric—of which there are potentially many in crude oil-related samples. In addition, FT-ICR MS has, like any

analytical technique, some limitations—such as the timescale for data acquisitions, which can be prohibitively long in some circumstances. FT-ICR MS instruments are very expensive, and there is the chance of encountering ion discrimination due to charge effects within the ion cloud formed in the instrument. Ideally, the analysis of complex mixtures, like crude oil and related samples, would be accomplished using a range of complementary analytical tools. One such complementary tool is ion mobility spectrometry (IMS), which, when coupled with mass spectrometry (MS), offers an orthogonal separation technique based on the mass, size, shape, and charge of the components in the sample. The shape of a molecule can lead to its stereochemistry, and hence the utilisation of IMS-MS offers new possibilities for the optimisation (via kinetic modelling) of crude oil conversion and hydrotreatment processes. For example, the efficiency of catalytic processing can depend upon the degree to which the components of the feedstock interact with the active phase of the catalyst as they pass through the catalyst's pores. An understanding of both the catalyst porosity and the molecular size distribution within the feedstock potentially offers important information for the design and development of new catalysts.

The development and utilisation of ion mobility-mass spectrometry (IMS-MS) has proceeded apace since its inception in the early 1960s by E. W. McDaniel—described by some as "the father of ion mobility-mass spectrometry" [14]. Ion mobility is a well established technique, and ion mobility instrumentation can take several forms, comprehensive descriptions of which may be found in the text by Eiceman and Karpas [15]. One more recently developed manifestation of ion mobility is Travelling Wave Ion Mobility Spectrometry (TWIMS), which uses sequential DC pulses across a series of ring electrodes to bring about the ion mobility separation [16–20].

Ion mobility has found use in a diverse range of applications covering many fields of scientific research. A large proportion of applications relate to the life sciences, such as the analysis of proteins and peptides [17, 21–23], or saccharides and related molecules [24–27], and has proved particularly useful for investigating structural isomers [28, 29]. Other selected applications include the analysis of chemical warfare agents [30, 31], pesticides [32, 33], explosives [34], and the analysis of drugs—both pharmaceutical [35–37] and illicit [38]. The applicability of IMS to chiral separation has also been demonstrated [39], and it has found particular utility in polymer analysis [40–44]. Significantly, there has been growing interest in the use of IMS in oil and petroleum analysis [45–47] to assist in the deconvolution of complex samples and provide additional component resolution. In this work we consider some examples of how IMS can be utilised in addressing the challenges faced in crude oil and petroleum analysis; along with complementary information that can be gained in relation to size distribution of species within samples, with reference to how this could be significant in catalyst design and development.

Experimental

Instrumentation and data handling

The FT-ICR MS analyses were carried out using a 7 Tesla LTQ FT Ultra (Thermo, Bremen, Germany) equipped with the Ion Max ESI ion source—henceforth referred to as FT MS. The travelling wave ion mobility separation was carried out using a SYNAPT G2 HDMS mass spectrometer (Waters Corporation, Manchester, UK), which has a quadrupole/travelling wave ion mobility/time-of-flight geometry with electrospray ionisation—henceforth referred to as TWIMS MS (Fig. 1).

The ion mobility region of the mass spectrometer comprises three sequential travelling wave regions, together known as a Triwave (Fig. 2). The structure and operating principles of the Triwave and travelling wave ion mobility have been described in detail elsewhere [16, 17, 19]. However, in brief, ions pass from the quadrupole and enter into a trapping area, where they are gated and released into the mobility drift region in packets. The mobility region is typically filled with nitrogen gas, and the ions first pass through a helium cell at the front of the mobility region—the helium cell is on the left side of the IMS section in Fig. 2. This helium cell increases the efficiency of transmission of ions into the mobility region and kinetically cools the ions to reduce any possible fragmentation that may occur as they pass into this higher pressure region. In the IMS region, ions are separated according to their mobilities using travelling waves and then exit into a third t-wave section that transfers the separated ions into the time-of-flight analyser. Each travelling wave section utilises a stacked-ring ion guide, across which a repeat sequence of pulsed voltages is applied. The ions, effectively, "surf" on the wave front of these voltages, and are transported through the instrument. Importantly, in the ion mobility region, the less mobile ions are overtaken by the wave more often than the more mobile ions - thus effecting mobility separation of the ions.

Use of TWIMS MS for calculating collision cross sections (CCS) relies upon accurate calibration of the travelling wave mobility cell [37, 48, 49]. This was carried out using polyalanine solution, ensuring that exactly identical instrument settings were used for the calibration acquisition as were used for acquisition of analyte data. Calibration of the mobility cell is required to ensure that drift times measured with TWIMS and nitrogen as the mobility gas can be related to absolute size measurements obtained from drift tube ion mobility instruments with helium as the mobility gas. Calibrations using previously measured species, such as polyalanine used in this work, have been demonstrated to generate accurate absolute size measurements from TWIMS instruments [50]. In addition, calibration of the ToF MS was carried out using sodium formate solution prior to the analyses. Mass accuracy of each acquisition was further ensured by implementation of an external lockmass: leucine enkephalin,
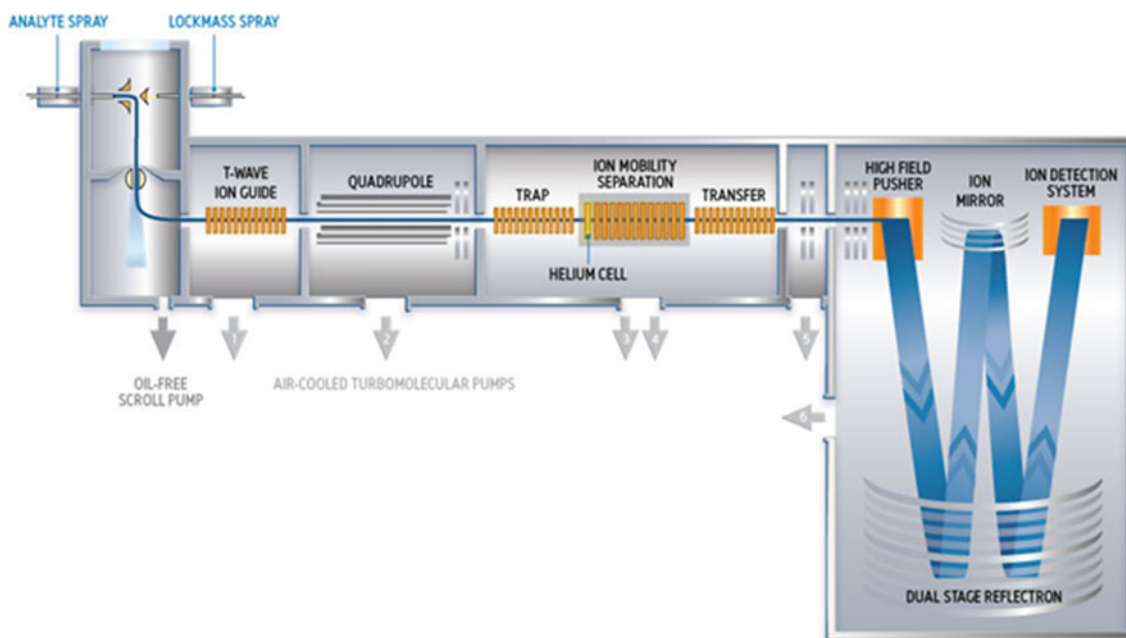
**Fig. 1** Schematic of the SYNAPT G2 HDMS mass spectrometer

556.2771 *m/z* for positive ion mode. The analyses were carried out with a typical mass resolving power for the ToF of ~30000 at 400 *m/z* (full width at half-maximum of the peak height).

The ion mobility and ToF MS experimental conditions were as follows: trap collision energy (CE), 4.0 V; transfer CE, 0.0 V; argon trap/transfer collision gas flow, 2.5 mL/min; helium cell gas flow, 180 mL/min; nitrogen IMS gas flow, 110 mL/min; resulting IMS cell pressure, 3.5 mbar; IMS travelling wave height/velocity, 40.0 V/1200 m/s; ToF acquisition mass range, 100–1000 *m/z*. The electrospray ion source-specific conditions were: capillary voltage, 3.8 kV; sample cone, 30 V; source temperature, 120 °C; desolvation temperature, 250 °C; nitrogen cone gas flow, 20 L/Hr, nitrogen desolvation gas flow, 400 L/Hr. Solutions of the resin sample

were introduced into the ESI source via direct infusion at a flow rate of 10 μL/min; no chromatographic separations were used. Total acquisition time: 5 min.

Instrument control and data acquisition were carried out using MassLynx v4.1 (Waters Corporation, Milford, MA, USA); ion mobility data were viewed and processed in ion mobility-specific software, DriftScope v2.2 (Waters Corporation, Manchester, UK). Lists of detected mass and ion mobility peaks can be exported from DriftScope in various file formats, for use with other software packages. In this work, ion mobility peak detection lists were exported in Excel spreadsheet format for import into bespoke, in-house Kendrick plot software at IFP Energies nouvelles (IFPEN) (Lyon, France).

Fig. 2 Diagram of the Triwave region of the mass spectrometer
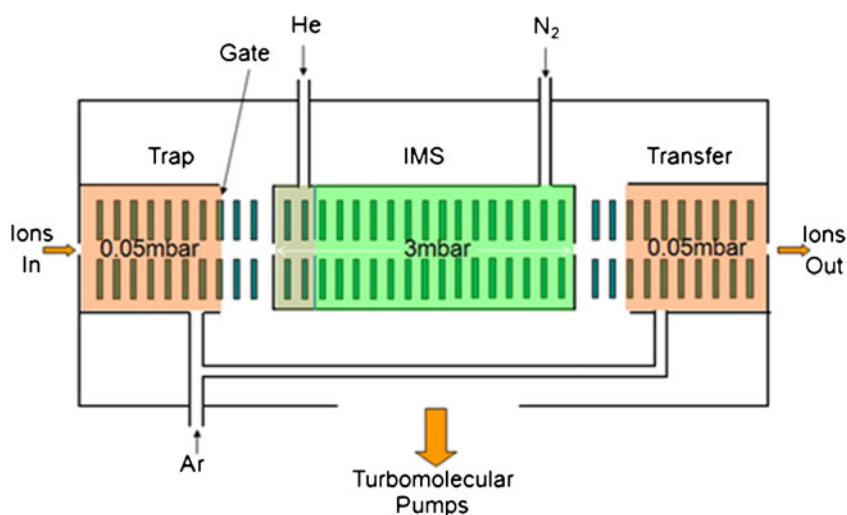
FT MS analyses were carried out with a resolving power of 100 000 FWHM at $400 \, m/z$ with the following experimental conditions: acquisition mass range 100–1000 m/z; automatic gain control (AGC) enabled; ICR ion target, 1×10^5; mass spectra averaging (μscans), 128. ESI ion source settings were set as follows: source voltage, 3.8 kV; nitrogen sheath gas flow rate, 6 (Arb. Unit); nitrogen aux gas, 2; capillary voltage, 20 V; tube lens voltage, 100 V; capillary temperature, 250 °C; syringe pump flow rate, 5 μL/min. Instrument control and data acquisition were carried out using respectively LTQ Ultra 2.5.5 (Thermo, Bremen Germany) and Qual Browser 2.0.7 from the Xcalibur suite (Thermo, Bremen, Germany). Automatic data treatment was performed with in-house Kendrick plot software at IFPEN [10].

Sample preparation

All solvents, of HPLC grade or better, were purchased from Sigma Aldrich (Dorset, UK) and used without further purification. A sample of the resins portion of the Saturates, Aromatics, Resins, and Asphaltenes (SARA) fraction of crude oil obtained from the Nigerian Egina oil field was provided by IFPEN. Portions of this sample were dissolved in 1:1 toluene: methanol with 0.1 % formic acid, for analysis by FT MS. Calmix (Caffeine, MRFA peptide and Ultramark), used as the external lockmass for FT MS, was purchased from Sigma Aldrich (St Quentin Fallavier, France). The resins sample was dissolved in 1:1 toluene:methanol for analysis by TWIMS MS. Sodium formate and polyalanine, used for instrument calibration, and leucine enkephalin, used as the external lockmass for TWIMS MS, were each purchased from Sigma Aldrich (Dorset, UK).

Results & discussion

Solutions of the Egina resin sample were analysed as described in the Experimental section. Figure 3 shows a typical ToF MS spectrum for the resin sample, along with the corresponding two dimensional drift time versus m/z image, expanded to cover the range 100–500 m/z—the mass range in which the majority of ions can be found. A peak detection algorithm has been applied to the data to help distinguish both mass resolved and mobility resolved species. The
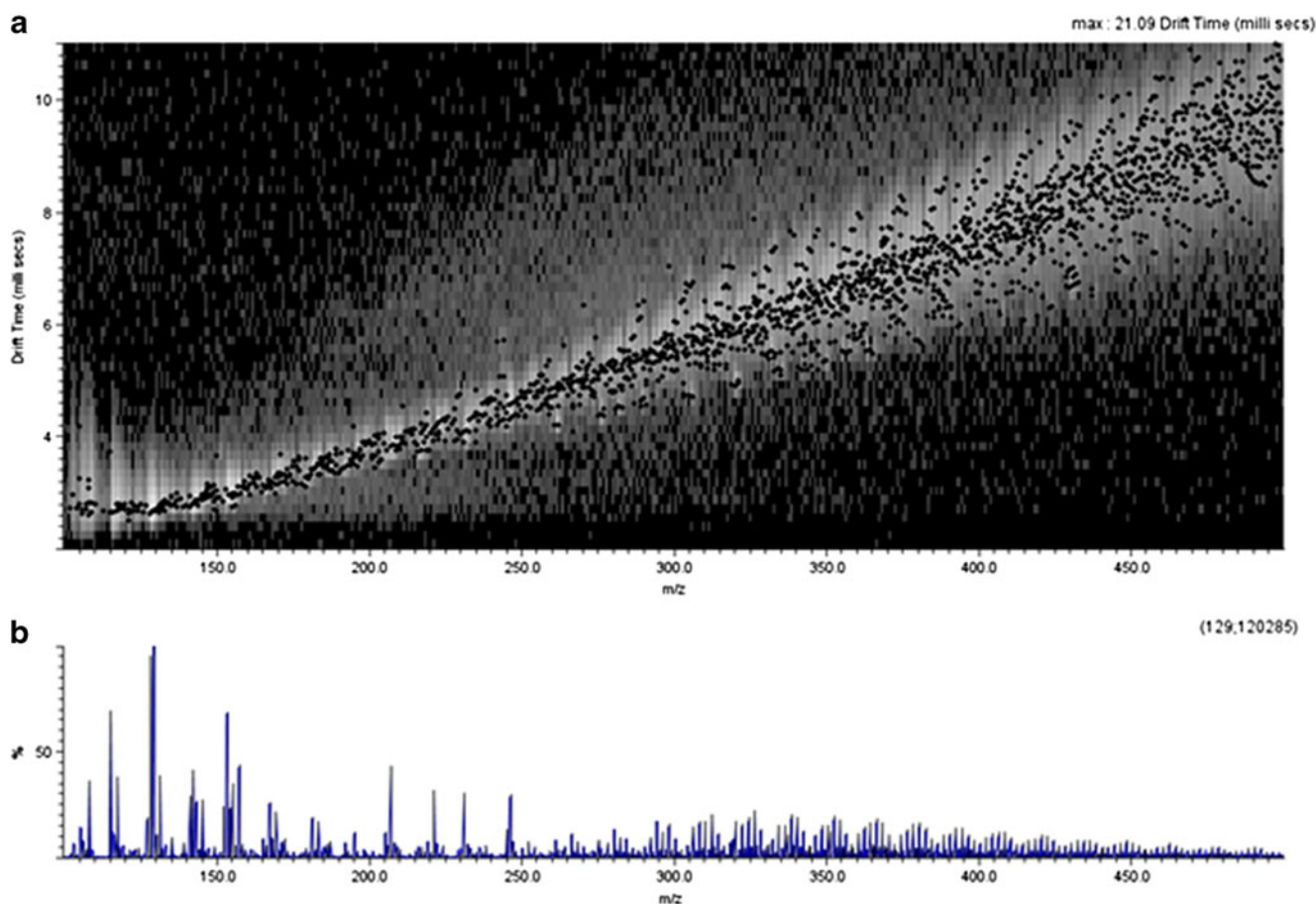

Fig. 3 Typical two dimensional drift time versus m/z mobility image and spectrum for Egina resin sample acquired using TWIMS MS. **a** peak detected 2D mobility image, **b** peak detected mass spectrum
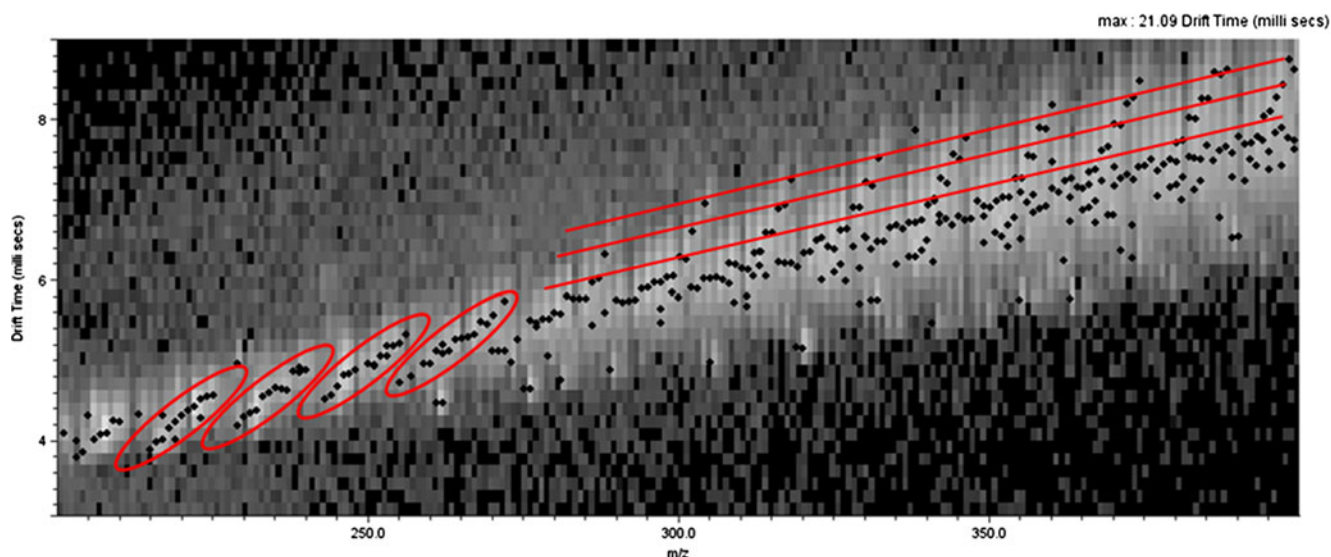
Fig. 4 The two dimensional drift time versus *m/z* mobility image for an Egina resin sample shows a high degree of order within both the short and long diagonals

application of threshold values to detected peaks in the mobility image helped to visualise clear patterns and groups, or series, of related species, as shown in Fig. 4. It was observed that the mobility separated ions show very ordered distributions along both short diagonals, where the significant mass difference is 2 Da—corresponding to a 2H change (circled in Fig. 4); and long diagonals, where the significant mass difference is 14 Da—corresponding to a CH_2 unit change (highlighted by lines in Fig. 4). These patterns bear a strong resemblance to the types of ordered information seen in many tools used to visualise and evaluate crude oil data, for example, Kendrick plots.

Patterns within the ion mobility data were explored further by using, in the first instance, the acquired masses and intensities without considering the mobility separation. A

detected peak list, with a low detection threshold to ensure full coverage, was exported from DriftScope in CSV file format. These data were transformed into Kendrick plots using in-house software at IFPEN. This software enabled the automatic selection and identification of a family (ions with the same heteroatomic composition) with the exact mass measurement only. In a first attempt, a mass tolerance of 5 ppm was set. Figure 5 illustrates the Kendrick plot for a nitrogen-containing family, generated using TWIMS MS data. While the Kendrick plot generated using these data looks broadly similar to Kendrick plots generated from FT MS data (Fig. 6), it was noticed that, in some places, the lines are less straight than those seen in Kendrick plots generated from FT MS data—for example in the region circled in Fig. 5. This could be due to the complexity of
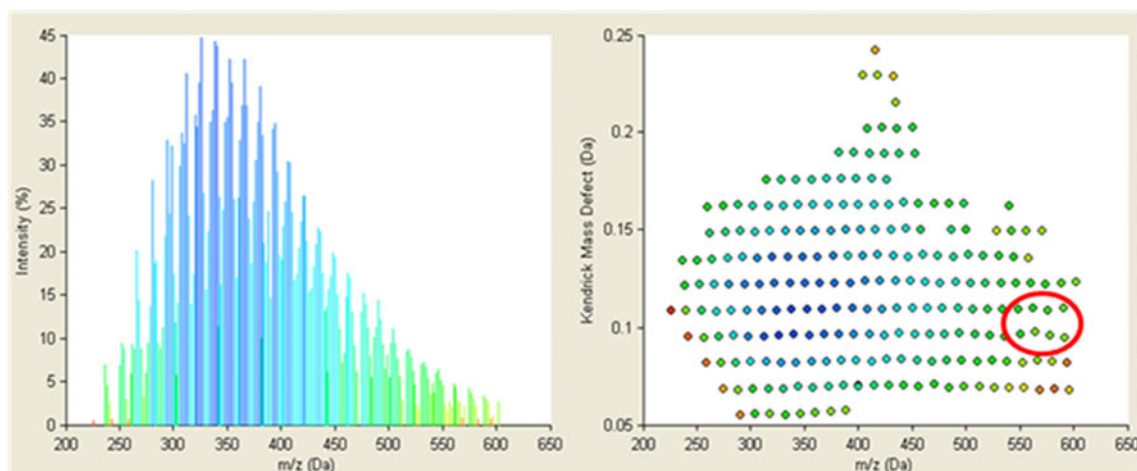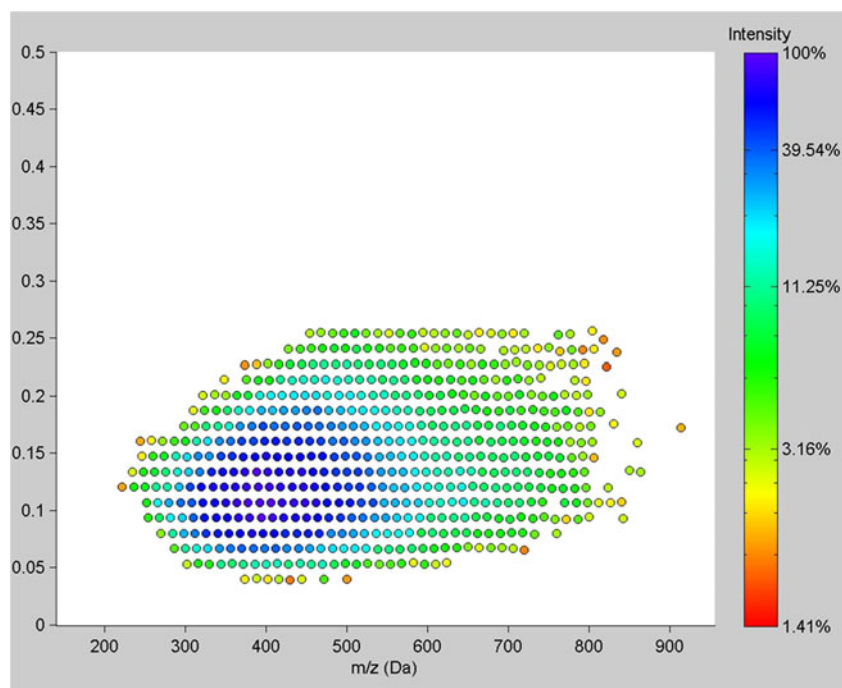

Fig. 5 Spectrum of a nitrogen-containing group in the resin sample with the associated Kendrick plot generated from TWIMS MS data. A region where the lines are less straight than those seen with FT MS data is circled on the Kendrick plot

Fig. 6 Kendrick plot of a nitrogen-containing group in the resin sample generated from FT MS data

the sample which created unresolved interferences and less accurate mass measurements when using a QToF MS compared with the very high mass resolution achievable with an FT MS. The data were then reviewed to evaluate how the limitations of comparatively lower mass resolution may be overcome by inclusion of the ion mobility data points. It was observed that species that belong to the same heteroatom family do not only have sequences of recognisable mass
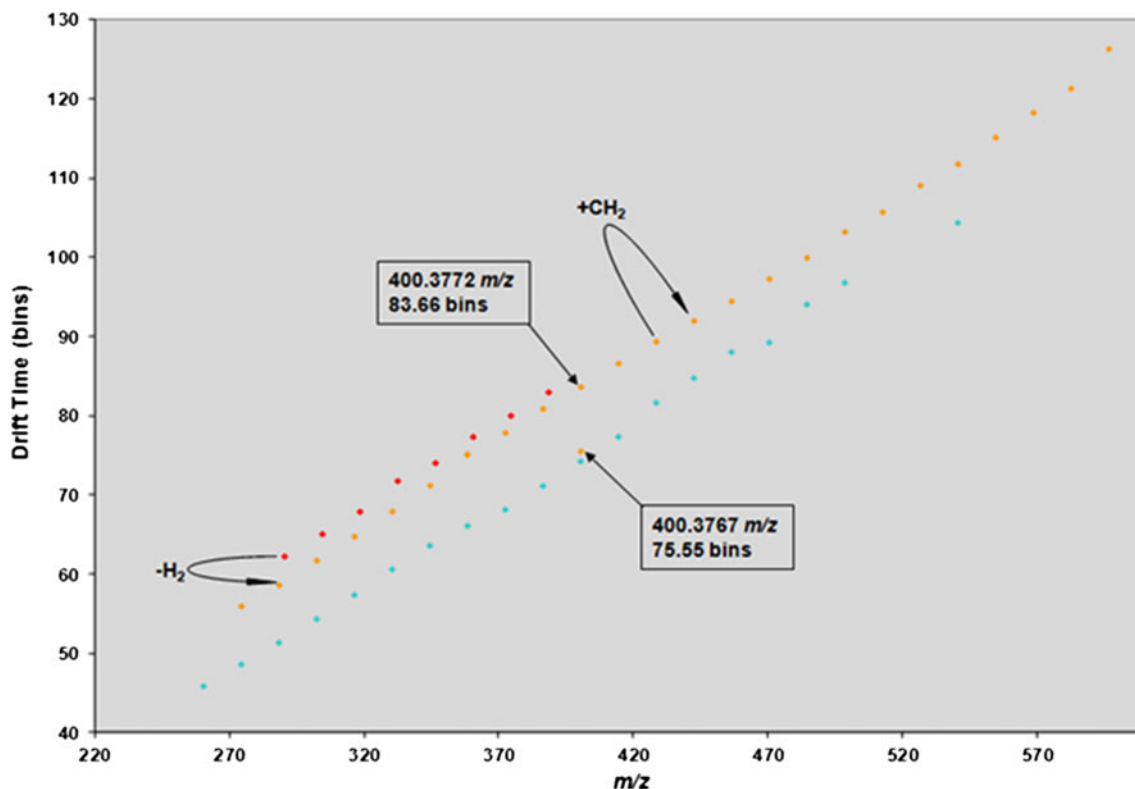

Fig. 7 A plot of drift time versus *m/z* showing three different DBE series for one particular nitrogen-containing family. Consideration of the ion mobility data helped to isolate an incorrectly assigned ion when selection was based on mass-to-charge ratio alone

differences, such as that corresponding to CH_2 for carbon number series, or H_2 for double bond equivalence (DBE), but also appear to lie along straight lines within the mobility images. This is presumed to be due to the fact that, typically in ion mobility acquisitions, incremental changes in structure produce similar incremental changes in drift times in a linear fashion, based on previous experimental observations.

Various nitrogen-containing series were identified within the peak list exported from DriftScope, by comparing the acquired QToF MS masses with those previously acquired using FT MS (data not shown here). One such nitrogen-containing family was then isolated and plotted as drift time against mass-to-charge ratio, for various series with DBE of 0–12 and carbon numbers 13–40. Figure 7 shows three of the DBE series for this nitrogen-containing family, which correlate with the long diagonals in the mobility image. The difference between the long diagonal lines correspond to the mass difference for -H_2, or an increase of one double bond, moving down the plot towards the x-axis. Interestingly, inclusion of the mobility data enabled the discovery of an incorrect assignment of a member of the DBE = 1 series that occurred when selection was based on mass alone. In the centre of the plot, the ion $400.3767 \, m/z$ was selected by the software as being a member of the DBE = 1 series, based on its acquired mass-to-charge ratio. However, when this ion was plotted with its drift time it was clear that this ion was not a member of the DBE = 1 series because it did not fall on the

long diagonal for DBE = 1. In fact, the ion $400.3772 \, m/z$ is the correct member of the series as its ion lies exactly at the expected drift time for a member of the DBE = 1 series.

A similar analysis was also done for carbon number. Figure 8 shows the same nitrogen-containing family plotted as drift time against mass-to-charge ratio, coloured to highlight the carbon number series along the short diagonal lines. In this case, the difference between related series corresponds to the mass of a CH_2 unit, and increasing carbon number moving upwards and to the right along the plot. Also shown in Fig. 8 is a further illustration of an erroneous assignment of a series member for the C_{28} series. In this example, the ion mobility information, once again, helped to overcome the selection of an incorrect ion based on its mass-to-charge ratio alone. It appears that all the required information for the generation of a Kendrick plot was contained inside the ion mobility drift time plot. Moreover, thanks to the drift time measurement, it was possible to compensate for the lower resolution and mass accuracy of TWIMS in comparison with FT MS.

In addition, application of the polyalanine ion mobility calibration to the data set enabled a detailed evaluation of the size, or CCS, of the species of interest. Measurement of the size distribution across different heteroatom series of interest is unique information which is unobtainable by MS alone. It could prove extremely valuable in decision making related to novel catalyst design. The catalysts used
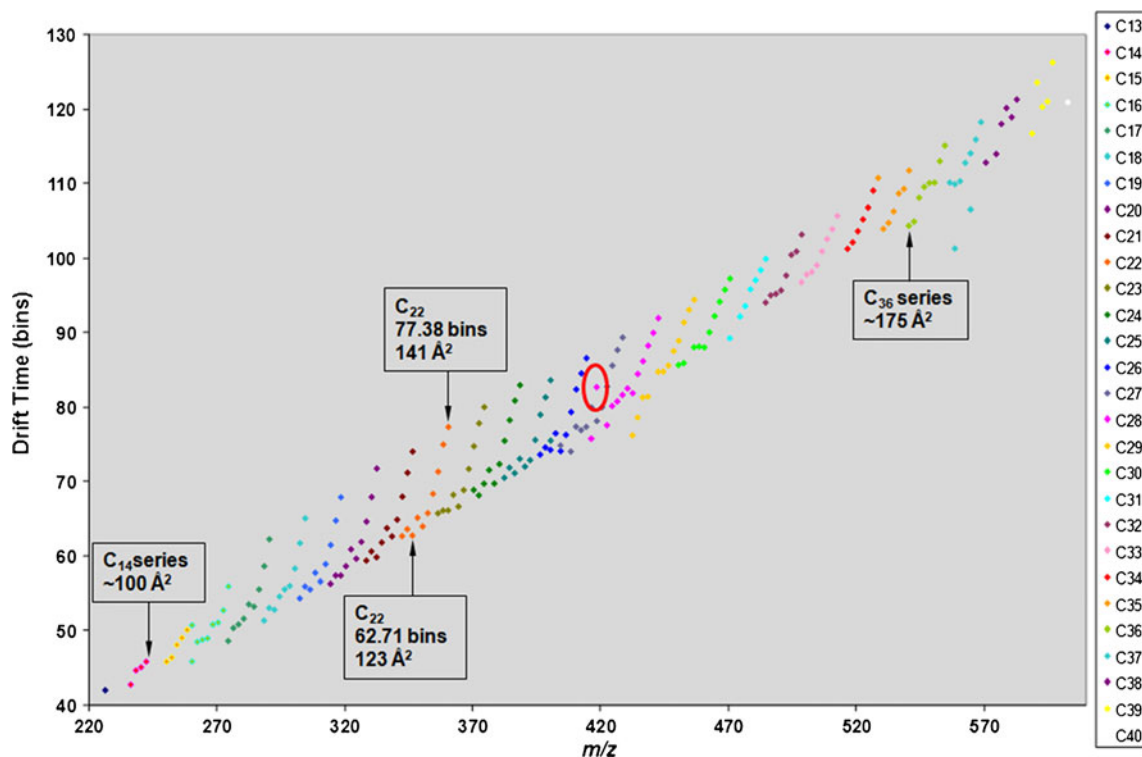

Fig. 8 The A plot of drift time versus m/z showing carbon number series for one particular nitrogen-containing family. Both an incorrectly assigned ion (*circled in red*) and the calculated sizes, based on measured collision cross sections, of certain components of the data are also shown

during different stages of oil processing are of vital importance in ensuring the quality of the products generated from crude oil [51]. The catalyst structures and porosity can be theoretically modelled, and can be studied using techniques such as 3-Dimensional Transmission Electron Microscopy (3D-TEM) [52]. This allows the calculation of the catalyst's pore size which are ranged in three categories after observations from unpublished experimental TEM measurements: (i) the micro porosity for diameters below 2 nm, (ii) the meso porosity for diameters from 2 nm to 50 nm and (iii) the macro porosity for diameters above 50 nm (from unpublished experimental measurements). If the absolute sizes of species that are required to be removed by catalytic processing are known, then catalyst pore sizes can be more precisely engineered to ensure the most efficient analyte-catalyst interactions by minimizing the diffusional limitations. The CCS information in Fig. 8 shows that as the carbon number increases the drift time gets longer, and hence the sizes of the species also increase—as would be expected with increasing carbon number. Furthermore, as the DBE, or aromaticity, of the species increase the drift times decrease—so a more aromatic species is more compact, thus giving an absolute measurement of the decrease in size as the species become increasingly aromatic. The analysis of Egina resins (Fig. 8) showed a C_{36} molecule with a CCS of 175 $Å^2$. Assuming that the molecule's shape is a disk, it corresponds to a diameter of 0.7 nm which is far below the micro porosity. Use of this approach enables the mapping of sizes for related species and classes of compounds within crude oil and similar samples. TWIMS was of considerable interest as it allowed the generation of a Kendrick plot enriched by the information of the molecular size.

Conclusion

The applicability and potential benefits of using ion mobility-mass spectrometry for the analysis of oil and petroleum samples has been examined. The resins portion of the SARA fractions of a Nigerian crude oil was used as a representative sample for analysis. When the ion mobility data were reviewed, clear, regular patterns were observed that were analogous to the patterns seen in typical graphical displays of crude oil data, such as Kendrick plots. The high resolution exact mass data from the SYNAPT HDMS instrument were used to generate Kendrick plots; however, the lower mass resolution compared with FT-ICR MS data resulted in less accurate plots. The inclusion of ion mobility information enabled the identification of several incorrect assignments of ions, which only became apparent when both mass and drift time were taken into consideration. This demonstrated the effectiveness of using ion mobility

data to aid in isolating and identifying important groups, or families, of related species within the data.

Calibration of the TWIMS region of the instrument using polyalanine allowed the calculation of the sizes of species within the sample. The implementation of ion mobility is the only way in which detailed information about the sizes and shapes of individual components of oil and petroleum samples can be obtained, while also obtaining mass to charge ratios and ion intensities when ion mobility is coupled with mass spectrometry. The value of knowledge about size distribution in oil and petroleum samples was recognised—particularly in relation to catalyst development. Ion mobility-mass spectrometry was found to offer useful, complementary information to that typically generated in the analysis of crude oil samples using FT-ICR MS. Ion mobility is, potentially, a powerful tool for future analyses in the oil and petroleum industry; and further work will examine its applicability in analysing other significant components of crude oil samples, such as asphaltenes and naphthenic acids.

References

1. Lumpkin HE, Johnson BH (1954) Anal Chem 26:1719–1722
2. Reid WK (1966) Anal Chem 38:445–449
3. Marshall AG, Rodgers RP (2003) Acc Chem Res 37:53–59
4. Rodgers RP, Schaub TM, Marshall AG (2005) Anal Chem 77:20 A–27 A
5. Marshall AG, Rodgers RP (2008) Proc Natl Acad Sci 105:18090–18095
6. Corilo YE, Vaz BG, Simas RC, Lopes Nascimento HD, Klitzke CF, Pereira RCL, Bastos WL, Santos Neto ENV, Rodgers RP, Eberlin MN (2012) Anal Chem 82:3990–3996
7. Klitzke CF, Corilo YE, Siek K, Binkley J, Patrick J, Eberlin MN (2012) Energy Fuel 26:5787–5794
8. Kendrick E (1963) Anal Chem 35:2146–2154
9. Hughey CA, Hendrickson CL, Rodgers RP, Marshall AG, Qian K (2001) Anal Chem 73:4676–4681
10. Chainet F, Ponthus J, Lienemann C-P, Courtiade M, Donard OFX (2012) Anal Chem 84:3998–4005
11. Comisarow MB, Marshall AG (1974) Chem Phys Lett 25:282–283
12. Hughey CA, Rodgers RP, Marshall AG (2002) Anal Chem 74:4145–4149
13. Kim S, Rodgers RP, Marshall AG (2006) Int J Mass Spectrom 251:260–265
14. Kanu AB, Dwivedi P, Tam M, Matz L, Hill HH (2008) J Mass Spectrom 43:1–22
15. Eiceman GA, Karasek FW (2004) Ion mobility spectrometry, 2nd edn. CRC Press, Boca Raton
16. Giles K, Pringle SD, Worthington KR, Little D, Wildgoose JL, Bateman RH (2004) Rapid Commun Mass Spectrom 18:2401–2414
17. Pringle SD, Giles K, Wildgoose JL, Williams JP, Slade SE, Thalassinos K, Bateman RH, Bowers MT, Scrivens JH (2007) Int J Mass Spectrom 261:1–12
18. Shvartsburg AA, Smith RD (2008) Anal Chem 80:9689–9699

19. Giles K, Wildgoose JL, Langridge DJ, Campuzano I (2010) Int J Mass Spectrom 298:10–16
20. Giles K, Williams JP, Campuzano I (2011) Rapid Commun Mass Spectrom 25:1559–1566
21. Beegle LW, Kanik I, Matz L, Hill HH Jr (2002) Int J Mass Spectrom 216:257–268
22. Ruotolo BT, Tate CC, Russell DH (2004) J Am Soc Mass Spectrom 15:870–878
23. Woods AS, Ugarov M, Egan T, Koomen J, Gillig KJ, Fuhrer K, Gonin M, Schultz JA (2004) Anal Chem 76:2187–2195
24. Lee S, Wyttenbach T, Bowers MT (1997) Int J Mass Spectrom Ion Process 167–168:605–614
25. Gabryelski W, Froese K (2003) J Am Soc Mass Spectrom 14:265–277
26. Clowers BH, Dwivedi P, Steiner WE, Hill HH, Bendiak B (2005) J Am Soc Mass Spectrom 16:660–669
27. Williams JP, Grabenauer M, Holland RJ, Carpenter CJ, Wormald MR, Giles K, Harvey DJ, Bateman RH, Scrivens JH, Bowers MT (2010) Int J Mass Spectrom 298:119–127
28. Wu C, Siems WF, Klasmeier J, Hill HH (1999) Anal Chem 72:391–395
29. Li H, Giles K, Bendiak B, Kaplan K, Siems WF, Hill HH (2012) Anal Chem 84:3231–3239
30. Steiner WE, Clowers BH, Matz LM, Siems WF, Hill HH (2002) Anal Chem 74:4343–4352
31. Makinen MA, Anttalainen OA, Sillanpaa MET (2010) Anal Chem 82:9594–9600
32. Borsdorf H, Roetering S, Nazarov E, Weickhardt C (2009) Int J Ion Mobil Spectrom 12:15–22
33. Weickhardt C, Kaiser N, Borsdorf H (2012) Int J Ion Mobil Spectrom 15:55–62
34. Crawford CL, Boudries H, Reda RJ, Roscioli KM, Kaplan KA, Siems WF, Hill HH (2009) Anal Chem 82:387–393
35. Eckers C, Laures AMF, Giles K, Major H, Pringle S (2007) Rapid Commun Mass Spectrom 21:1255–1263
36. Howdle MD, Eckers C, Laures AMF, Creaser CS (2010) Int J Mass Spectrom 298:72–77
37. Campuzano I, Bush MF, Robinson CV, Beaumont C, Richardson K, Kim H, Kim HI (2012) Anal Chem 84:1026–1033
38. Wu C, Siems WF, Hill HH (1999) Anal Chem 72:396–403
39. Dwivedi P, Wu C, Matz LM, Clowers BH, Siems WF, Hill HH (2006) Anal Chem 78:8200–8206
40. Jackson AT, Scrivens JH, Williams JP, Baker ES, Gidden J, Bowers MT (2004) Int J Mass Spectrom 238:287–297
41. Trimpin S, Plasencia M, Isailovic D, Clemmer DE (2007) Anal Chem 79:7965–7974
42. Bagal D, Zhang H, Schnier PD (2008) Anal Chem 80:2408–2418
43. Trimpin S, Clemmer DE (2008) Anal Chem 80:9073–9083
44. Barrere C, Maire F, Afonso C, Giusti P (2012) Anal Chem 84:9349–9354
45. Becker C, Qian K, Russell DH (2008) Anal Chem 80:8592–8597
46. Fernandez-Lima FA, Becker C, McKenna AM, Rodgers RP, Marshall AG, Russell DH (2009) Anal Chem 81:9941–9947
47. Ahmed A, Cho YJ, No M-H, Koh J, Tomczyk N, Giles K, Yoo JS, Kim S (2011) Anal Chem 83:77–83
48. Clemmer DE, Jarrold MF (1997) J Mass Spectrom 32:577–592
49. Smith DP, Knapman TW, Campuzano I, Malham RW, Berryman JT, Radford SE, Ashcroft AE (2009) Eur J Mass Spectrom 15:113–130
50. Thalassinos K, Grabenauer M, Slade SE, Hilton GR, Bowers MT, Scrivens JH (2009) Anal Chem 81:248–254
51. Absi-Halabi M, Stanislaus A, Al-Mughni T, Khan S, Qamra A (1995) Fuel 74:1211–1215
52. Ersen O, Hirlimann C, Drillon M, Werckmann J, Tihay F, Pham-Huu C, Crucifix C, Schultz P (2007) Solid State Sci 9:1088–1098